Underwater ghost imaging with pseudo-Bessel-ring modulation pattern

Zhe Sun (孙 哲)[1,†], Tong Tian (田 通)[2,3,†], Sukyoon Oh[2,3], Jiang Wang (王 江)[1], Guanghua Cheng (程光华)[1*], and Xuelong Li (李学龙)[1**]

[1] School of Artificial Intelligence, Optics and Electronics (iOPEN), Northwestern Polytechnical University, Xi'an 710072, China
[2] Institute of Optics and Quantum Electronics, Abbe Center of Photonics, Friedrich Schiller University, 07743 Jena, Germany
[3] Helmholtz Institute Jena, 07743 Jena, Germany

*Corresponding author: guanghuacheng@nwpu.edu.cn
**Corresponding author: li@nwpu.edu.cn

In this study, we propose an underwater ghost-imaging scheme using a modulation pattern combining offset-position pseudo-Bessel-ring (OPBR) and random binary (RB) speckle pattern illumination. We design the experiments based on modulation rules to order the OPBR speckle patterns. We retrieve ghost images by OPBR beam with different modulation speckle sizes. The obtained ghost images have a better contrast-to-noise rate compared to RB beam ghost imaging under the same conditions. We verify the results both in the experiment and simulation. In addition, we also check the image quality at different turbidities. Furthermore, we demonstrate that the OPBR speckle pattern also provides better image quality in other objects. The proposed method promises wide applications in highly scattering media, atmosphere, turbid water, etc.

1. Introduction

Underwater imaging technology plays an essential function in resource development and underwater object detection. To reduce the impact of distortion and loss in underwater imaging, ghost imaging has become one of the important research directions of long-distance underwater imaging[1–3] because it requires only one-dimensional intensity fluctuation information of the imaging object with good noise resistance. In 1995, Pittman et al.[4] first realized ghost imaging based on the theory of Klyshko[5,6] by generating spatially entangled photon pairs with spontaneous parametric downconversion. In 2002, Bennink et al. demonstrated that nonentangled thermal light sources could also be employed to achieve ghost imaging[7]. In 2008, Shapiro[8] proposed a theory of computational ghost imaging capable of omitting the reference optical path. A spatial light modulator (SLM) or a digital micromirror device (DMD) can directly generate a prefabricated modulated optical field, then receive the total light intensity by a bucket detector. Additionally, computational ghost imaging has played a more prominent role in advanced light-field modulation techniques[9,10].

Turbulence is a serious problem with classical imaging. Underwater optical imaging has to combat turbulence induced by temperature and salinity fluctuations. Surprisingly, the fluctuation index disturbance introduced in the optical path can be incorporated into the computational model in ghost imaging. Thus, ghost imaging is capable of effectively reducing the effect of atmospheric turbulence[11–14]. Similarly, applying ghost-imaging techniques to address turbulence in water has also received attention[15–24]. This property of ghost imaging is a historic milestone in optical imaging. However, as the propagation distance increases, the attenuation of the light field in the water becomes impossible to ignore[25–27]. Moreover, the computational models are no longer adaptable in practice. Even now, it is crucial to perform high-quality ghost imaging in water, although light-field attenuation remains challenging.

Fortunately, the Bessel beam provides a promising solution for light-field modulation to reduce attenuation. It can be mathematically formulated by the Bessel function, which is the solution of the Helmholtz equation in cylindrical coordinates[28]. The Bessel beam has a unique transverse toroidal pattern that does not change when it propagates over a certain distance[29], thus it is considered diffraction-free propagation and "self-healing." Therefore, Bessel beams can propagate in water with fewer diffraction scattering effects. In practice, a Bessel beam can be generated using a Gaussian beam coupled with an

axicon[30]. In addition, SLM[31] and DMD[32] can also be used to generate Bessel beams. In ghost imaging, Meyers *et al.*[15] first reported the use of a constantly shifted Bessel light field to overcome the influence of turbulence. However, this would generate strong background noise in the reconstructed image and degrade the imaging quality. Therefore, it is crucial to solve the problem of image quality degradation when utilizing Bessel beams for long-distance ghosting imaging in water.

In this work, we proposed the use of lateral Bessel rings with random intensity modulation to form an offset-position pseudo-Bessel-ring (OPBR) speckle pattern. We experimentally studied the influence of the different modulations of OPBR speckle pattern projection on the contrast-to-noise rate (CNR) of the retrieved ghost images in the digital micromirror device (DMD)-based computational ghost-imaging system. We ran a simulation in ideal conditions to verify the feasibility of the proposed method. Our results show that using the OPBR speckle pattern can effectively improve image quality compared to traditional ghost imaging. This method is very promising for high-quality ghost imaging in turbid water and can be easily applied to SLM-based computational ghost imaging, and axicon-based pseudothermal ghost imaging to replicate the properties of a Bessel beam.

2. Principle of Ghost-Imaging Reconstruction and Experimental Setup

Normally, it is hard to achieve excellent imaging performance in the underwater environment[25–27]. In order to enhance the ghost-image quality, we adopted a time-corrected algorithm for the ghost-imaging reconstruction. The DMD will randomly modulate and project different illuminations of OPBR speckle patterns $I(\vec{p})$ in our ghost-imaging system. The retrieved ghost image $G(\vec{p})$ can be reconstructed from the OPBR speckle patterns and single-pixel intensity B by a temporal corrected algorithm[33],

$$G(\vec{p}) = \left\langle (I(\vec{p}) - \langle I(\vec{p}) \rangle) \left(\frac{B_i}{B_{i-1}} - \left\langle \frac{B_i}{B_{i-1}} \right\rangle \right) \right\rangle, \quad (1)$$

where i is the iteration number, $i = 1, 2, 3, \ldots$, with $B_0 = 1$. The B_i are collected by the bucket detector, which is the summated intensity of transmitted light. "$\langle \rangle$" refers to the mean value by averaging operation. The ghost image can be calculated by correlation computation.

Generally, the time interval between two adjacent iterations can be very short in ghost imaging. The turbulence and scattering in the water can be approximated as constants during this very short time interval. Thus, the correlation with the ratio of the single-pixel values obtained from two adjacent iterations can eliminate the perturbation of the propagation scattering medium well.

We utilized nephelometric turbidity units (NTUs) to qualify water turbidity. The water turbidity is measured by its light transmission. Water becomes turbid, that is, less translucent,

because of the suspended particles it contains[34]. Here, we quantitatively evaluated the retrieved ghost-image quality by the CNR. Normally, the CNR is calculated from the signal and background intensity, then normalized to the noise[35,36],

$$\text{CNR} = \frac{\langle I_o \rangle - \langle I_b \rangle}{\sigma_{\text{GI}}}, \quad (2)$$

where $\langle I_o \rangle$ is the averaged signal value of the object, $\langle I_b \rangle$ is the averaged signal value of the background, and σ_{GI} is the standard derivation of the ghost image with noises. CNR can be helpful to distinguish between underwater object signals and background noise.

To experimentally verify the proposed method, the implementation setup was built as sketched in Fig. 1. A 10 mW laser beam with a wavelength of 532 nm, which is less absorbable to water, was used. We sequentially displayed a set of digitally OPBR speckle patterns on DMD and laser beam modulated accordingly in spatial intensity distribution. It should be noted that the micromirrors of DMD are 1280×800 with a pitch of 10.6 µm. The modulated beam propagates through the water tank and then falls on the object. To demonstrate the feasibility and performance of OPBR speckle patterns, a laser-cut transmitting digit "3" was prepared as the object. The actual profile of objects is shown in Fig. 1. The digit 3 was employed as an object because it contains the frequencies of all directions, and it is thus more representative. We also present an image of the digit 3 taken with a high-gain camera for comparison in Fig. 1. The transmitted light intensity was collected by a bucket detector. The computer was used to control the ghost-imaging system, produce the OPBR speckle patterns, control the patterns exhibition, record the light intensity data, and reconstruct the images. The shape of the object can be calculated by the correlation of the speckle pattern and the single-pixel intensity, which is indicated in Eq. (1). The retrieved ghost image was
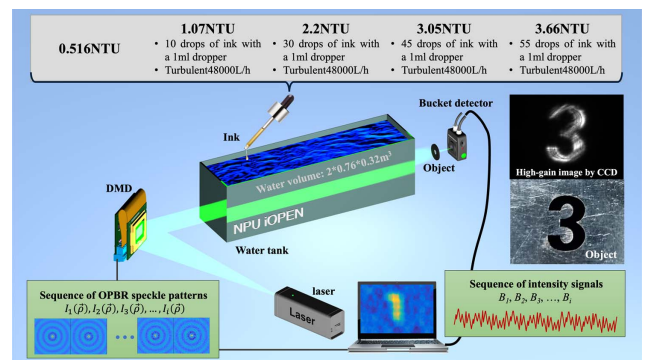

Fig. 1. Schematics of computational ghost imaging setup with the OPBR speckle patterns. A laser beam incidents on a DMD modulated by a sequence of RB speckle patterns. The modulated light propagates through turbid water and then falls on the object. The collected intensity fluctuation from the bucket detector can be used to retrieve the image by a second-order correlation algorithm. The volume of the water in the tank is 2 m × 0.76 m × 1 m.

reconstructed by the correlation of the intensity signals and the sequenced random binary (RB) speckle patterns.

3. Experimental Results and Discussion

To study the relation and regularity of the OPBR speckle pattern, we designed five sequences with different modulation speckles based on the Bessel function of the first kind. The five groups with 1500 speckle patterns were applied in the experiment for the robustness of this method. In this way, the sequenced OPBR speckle patterns are generated using different speckle sizes to modulate the offset-position Bessel-ring patterns (OBR), as shown in Fig. 2. A perfect Bessel beam fitting the mathematical description is not feasible, for it requires an infinitely large light field, and infinite intensity[28,29]. In some cases, the generated Bessel beams are inefficient and the propagation distances are limited[28–30]. In order to make a better application of the spatial properties of the Bessel beam, we adopted a DMD to modulate the incident beam into the shape of an offset-position Bessel beam with random speckles (here, the OPBR speckle patterns). It is worth noting that we utilized MATLAB to generate a mathematically 2D Bessel function. Then we extracted the ring-shaped structure of the generated function and loaded it to the DMD. The DMD chipset is DLP650L from ViALUX GmbH. The DMD pixel size used was 10.6 μm, with a modulation rate of 10,752 Hz. The data acquisition card supported 8-bit depth sampling. The single-pixel detector used had a detection band in the visible light range.

To test the effectiveness of the OPBR speckle patterns for image reconstruction in the scattering medium, we carried out experiments with the digit 3 object and estimated the CNR as the most significant measure for the image quality in the clear water (0.517 NTU). In Fig. 3, the upper half is the comparison of CNR values of different speckle sizes together with five sequences. The bottom half is the retrieved ghost images,
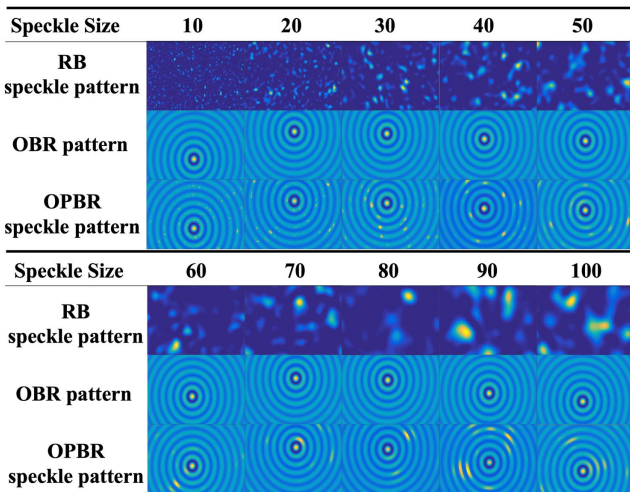

Fig. 2. The generation of the OPBR speckle patterns with different modulation speckles. The projection speckle size on DMD equals 10.6 μm × speckle size.
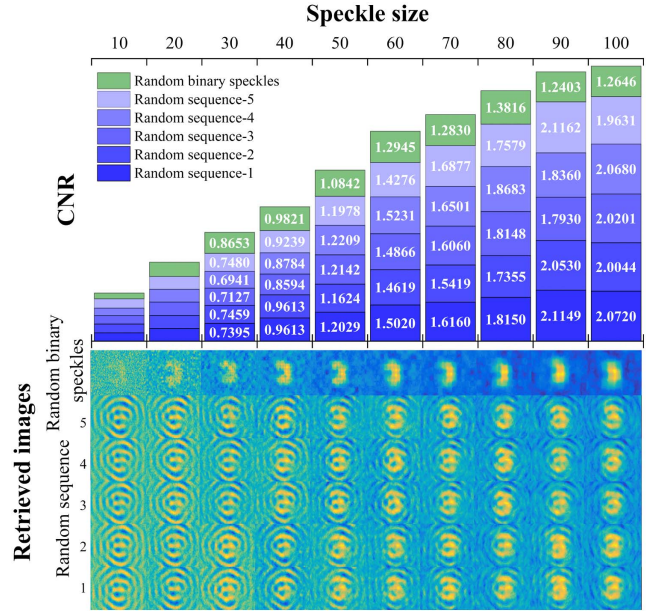

Fig. 3. Results for the retrieved image of the object of digit 3. Retrieved images and corresponding CNRs by the RB speckle patterns and the OPBR speckle patterns with different speckle sizes in the clear water (0.517 NTU). The upper part of the image shows the numerical comparison of CNR values, while the lower part shows the corresponding ghost-imaging results obtained. Each row represents the speckle imaging results obtained using the same type of speckle patterns but with different sizes, while each column represents the results obtained using the same size but with different types of speckle patterns. The projection speckle size on DMD equals 10.6 μm × speckle size.

which provide an intuitive way to compare imaging performance. The abscissas correspond to the variation of speckle sizes. The corresponding speckle size starts at 10 and gradually increases to 100 with steps of 10. The projection speckle size on DMD is the micromirror's pitch (10.6 μm) multiplied by the corresponding speckle size. The CNR values correspond to the retrieved image of the bottom half.

From Fig. 3, it is visible that the five sequences of CNRs increase with the modulation speckle size based on the OPBR speckle pattern. Since the offset-position pseudo-Bessel-rings are persistent, only the center location is moving relatively. After 1500 iterations, pseudo-Bessel-ring-shaped background noise becomes apparent, especially for a smaller modulation speckle size. The retrieved ghost images show that with the increase of modulated speckle size, the background noise caused by the pseudo-Bessel-rings gradually weakens. In addition, the retrieved ghost images gradually become apparent. The best CNR is achieved when using a modulation speckle size of 90. Both from the visibility and CNR, the retrieved ghost-image quality using the OPBR speckle pattern is superior to the RB speckle pattern.

Besides this, we also demonstrated the repeatability with five sequences using the OPBR speckle patterns in Fig. 3. We found that the CNRs of the five sequences were very close, indicating that the experimental results are reproducible. For a better

understanding, we also presented the retrieved ghost images with random speckles. As we can see from the CNR marked with the green color, the growth of the CNR slows down as the speckle size increases, especially relative to the OPBR speckle pattern. Moreover, retrieved underwater ghost images show this difference more obviously. Underwater ghost imaging uses random speckles, and it has become impossible to distinguish the object image due to the scattering in the water.

Furthermore, we checked the CNR in different turbidities using different sequences of OPBR speckle patterns to verify the performance of the proposed method. The turbid water is produced by a certain amount of ink and turbulence of 48,000 L/h. The specific steps and corresponding turbidity can be seen in Fig. 1. We summarized the dependence of the CNR on OPBR speckle patterns with different speckle sizes, and corresponding typically retrieved images are shown in Fig. 4. As the water turbidity increases, the image quality gradually deteriorates. However, the trend of retrieved image quality always increases with the modulated speckle sizes. We also produced five sequences of OPBR speckle patterns to verify the robustness of this method. As we can see, the CNRs of ghost images are sensitive between each sequence in high-turbidity water, while the CNRs are close to each other in low turbidity. This indicates that the speckle patterns are more sensitive to scattering in high-turbidity water. In addition, the image quality deteriorates strongly at high turbidity because the laser power applied in the experiment was too low to transmit 2 m of the high-turbidity water.

To better generalize our observations in imaging the object of the digit 3, the experiment was repeated with two digits of "1" and "2" with the same speckles. Figure 5 shows the experimental results of the CNR for the two digits. The ghost images for the two digits are also retrieved by 1500 independent iterations of the corresponding speckle patterns. The CNR increases rapidly compared with the RB speckle patterns in Fig. 3. It can be
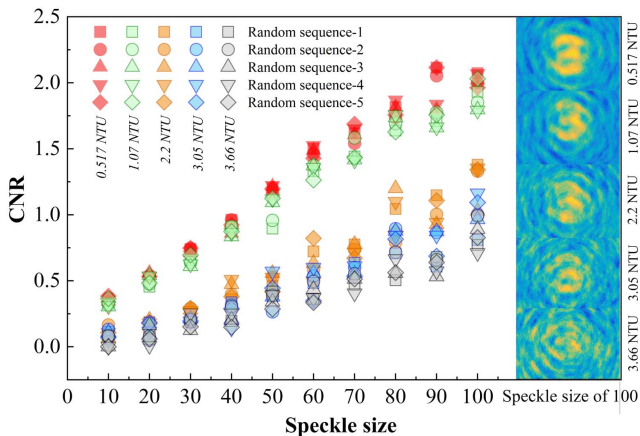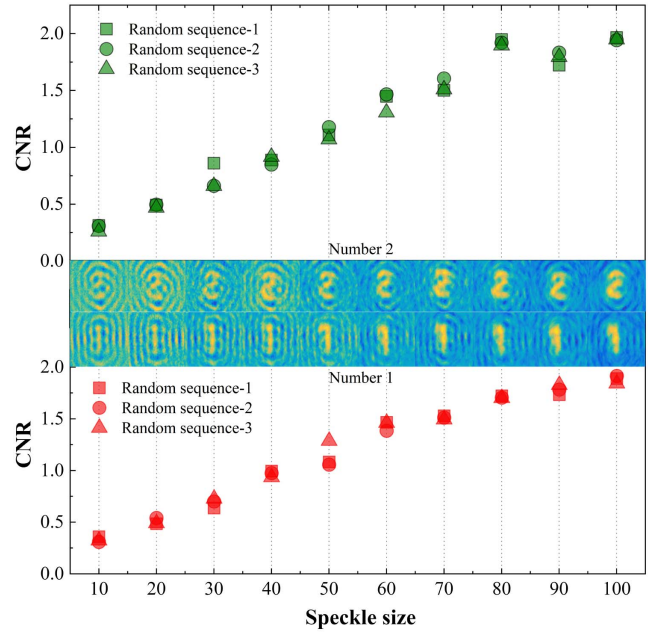

Fig. 5. The CNR by different OPBR speckle patterns for the object 1 and object 2 with different random sequences in the turbulent water. The projection speckle size on DMD equals 10.6 μm × speckle size.

concluded that the OPBR speckle patterns are applicable to objects with different shapes and still achieve better imaging quality. The agreement on the estimated quality of retrieved ghost images for the differently shaped objects with the same speckles is also excellent. A slight discrepancy was observed
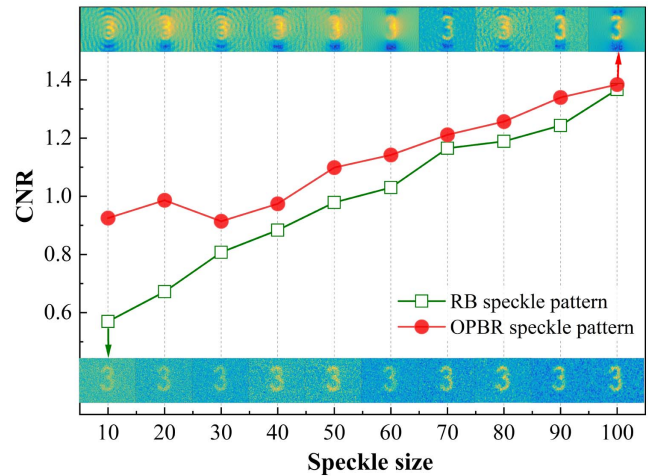

Fig. 4. The CNR by different OPBR speckle patterns with different sizes of speckles in turbid and turbulent water. The projection speckle size on DMD equals 10.6 μm × speckle size.

Fig. 6. Simulation results using the proposed OPBR speckle patterns and RB speckle patterns with a digit 3 object. The retrieved images by OPBR speckle patterns are presented at the top and the retrieved images by RB speckle patterns are presented at the bottom. The ghost images by RB speckle patterns of the digit 3 retrieve with the projection speckle size from 10.6 μm × 10 to 10.6 μm × 100. The proposed OPBR speckle patterns are modulated by the speckles with the speckle size from 10.6 μm × 10 to 10.6 μm × 100.

because of the deviation in the noise level for the corresponding speckle patterns for different object sizes[34].

In addition, we developed a simulation model to compare the simulation results with the experimental results described above. The RB speckle pattern and the OPBR speckle pattern employed the same speckle size. It can perform the simulation of different digit object reconstruction, ranging from speckle size of 10 to 100. In the simulation results, as shown in Fig. 6, the retrieved ghost images of the digit 3 with the same speckles are in good agreement with that in the experiments. In this case, the upper row in Fig. 6 shows the imaging results for RB speckle patterns, where the ghost imaging obtained by retrieval can barely distinguish the original object. In contrast, the imaging results incorporating the proposed OPBR speckle pattern are more readily discernible from the original object; the results are shown at the bottom of Fig. 6. Along with this, we calculated the CNRs of the simulation results. It is clear to see that the CNRs of retrieved ghost images by the OPBR speckle patterns are obviously higher than that by the traditional RB speckle patterns. Thus, the simulation results show that the OPBR speckle patterns are suitable for all samples to obtain a better CNR in the scattering medium.

4. Conclusion

We proposed a speckle modulation method that can increase the quality of underwater ghost imaging. We designed the OPBR speckle patterns and projected them to the DMD in the computational ghost-imaging system. From our experiments, we obtained the pseudo-Bessel-ring modulation rules for the CNR growth. For comparison, we also checked the image quality using traditional RB speckle patterns. The results show that the OPBR speckle patterns are more advantageous in highly scattering media. For the universality and robustness of this method, the CNR scaling is observed for three different digit objects with the same patterns. An analysis of our simulation unambiguously identified the OPBR speckle patterns for the increase in CNR. Both experiments and numerical simulations demonstrate that the proposed method can significantly improve the quality of ghost imaging in the scattering medium. In addition, the novel OPBR speckle patterns found in this research could be of great importance in future underwater ghost imaging in modulating the speckle patterns for better image quality.

Acknowledgement

†These authors contributed equally to this work.

References

1. B. I. Erkmen and J. H. Shapiro, "Ghost imaging: from quantum to classical to computational," Adv. Opt. Photon. **2**, 405 (2010).
2. G. M. Gibson, S. D. Johnson, and M. J. Padgett, "Single-pixel imaging 12 years on: a review," Opt. Express **28**, 28190 (2020).
3. Z. Sun, F. Tuitje, and C. Spielmann, "A review of high-resolution microscopic ghost imaging with low dose pseudothermal light," J. Microsc. **284**, 3 (2021).
4. T. B. Pittman, Y. H. Shih, D. V. Strekalov, and A. V. Sergienko, "Optical imaging by means of two-photon quantum entanglement," Phys. Rev. A **52**, R3429 (1995).
5. D. N. Klyshko, "A simple method of preparing pure states of an optical field, of implementing the Einstein–Podolsky–Rosen experiment, and of demonstrating the complementarity principle," Sov. Phys. Usp. **31**, 74 (1988).
6. M. H. Rubin, D. N. Klyshko, Y. H. Shih, and A. V. Sergienko, "Theory of two-photon entanglement in type-II optical parametric down-conversion," Phys. Rev. A **50**, 5122 (1994).
7. R. S. Bennink, S. J. Bentley, and R. W. Boyd, "'Two-photon' coincidence imaging with a classical source," Phys. Rev. Lett. **89**, 113601 (2002).
8. J. H. Shapiro, "Computational ghost imaging," Phys. Rev. A **78**, 061802 (2008).
9. M. P. Edgar, G. M. Gibson, and M. J. Padgett, "Principles and prospects for single-pixel imaging," Nat. Photonics **13**, 13 (2019).
10. Y. Cao, Y. Xiao, Z. Pan, L. Zhou, and W. Chen, "High-fidelity temporally-corrected transmission through dynamic smoke via pixel-to-plane data encoding," Opt. Express **30**, 36464 (2022).
11. J. Cheng, "Ghost imaging through turbulent atmosphere," Opt. Express **17**, 7916 (2009).
12. P. Zhang, W. Gong, X. Shen, and S. Han, "Correlated imaging through atmospheric turbulence," Phys. Rev. A **82**, 033817 (2010).
13. P. Dixon, G. A. Howland, K. W. C. Chan, C. O'Sullivan-Hale, B. Rodenburg, N. D. Hardy, J. H. Shapiro, D. S. Simon, A. V. Sergienko, R. W. Boyd, and J. C. Howell, "Quantum ghost imaging through turbulence," Phys. Rev. A **83**, 051803 (2011).
14. R. E. Meyers, K. S. Deacon, and Y. Shih, "Turbulence-free ghost imaging," Appl. Phys. Lett. **98**, 111115 (2011).
15. R. E. Meyers, K. S. Deacon, A. D. Tunick, and Y. Shih, "Virtual ghost imaging through turbulence and obscurants using Bessel beam illumination," Appl. Phys. Lett. **100**, 061126 (2012).
16. Y. Gao, X. Fu, and Y. Bai, "Ghost imaging in transparent liquid," J. Opt. **46**, 410 (2017).
17. M. Le, G. Wang, H. Zheng, J. Liu, Y. Zhou, and Z. Xu, "Underwater computational ghost imaging," Opt. Express **25**, 22859 (2017).
18. L. Qu, Y. Bai, Q. Shen, S. Nan, H. Li, and X. Fu, "The noise analysis of ghost imaging in transparent liquid," Opt. Quant. Electron. **49**, 234 (2017).
19. C. L. Luo, Z. L. Li, J. H. Xu, and Z. M. Liu, "Computational ghost imaging and ghost diffraction in turbulent ocean," Laser Phys. Lett. **15**, 125205 (2018).
20. M. Q. Yin, L. Wang, and S. M. Zhao, "Experimental demonstration of influence of underwater turbulence on ghost imaging," Chin. Phys. B **28**, 094201 (2019).
21. Q. W. Zhang, W. D. Li, K. Liu, L. W. Zhou, Z. M. Wang, and Y. J. Gu, "Effect of oceanic turbulence on the visibility of underwater ghost imaging," J. Opt. Soc. Am. A **36**, 397 (2019).
22. Y. Zhang, W. Li, H. Wu, Y. Chen, X. Su, Y. Xiao, Z. Wang, and Y. Gu, "High-visibility underwater ghost imaging in low illumination," Opt. Commun. **441**, 45 (2019).
23. Q. Chen, A. Mathai, X. Xu, and X. Wang, "A study into the effects of factors influencing an underwater, single-pixel imaging system's performance," Photonics **6**, 123 (2019).
24. X. Yang, Y. Liu, X. Mou, T. Hu, F. Yuan, and E. Cheng, "Imaging in turbid water based on a Hadamard single-pixel imaging system," Opt. Express **29**, 12010 (2021).
25. R. C. Smith and K. S. Baker, "Optical properties of the clearest natural waters (200–800 nm)," Appl. Opt. **20**, 177 (1981).
26. W. Gong and S. Han, "Correlated imaging in scattering media," Opt. Lett. **36**, 394 (2011).
27. K. B. Houcine, G. Brun, I. Verrier, L. Froehly, and C. Veillas, "High-resolution optical correlation imaging in a scattering medium," Opt. Lett. **26**, 1969 (2001).

28. J. Durnin, J. J. Miceli, Jr., and J. H. Eberly, "Diffraction-free beams," Phys. Rev. Lett. **58**, 1499 (1987).

29. Z. Bouchal, J. Wagner, and M. Chlup, "Self-reconstruction of a distorted non-diffracting beam," Opt. Commun. **151**, 207 (1998).

30. J. H. McLeod, "The axicon: a new type of optical element," J. Opt. Soc. Am. **44**, 592 (1954).

31. J. A. Davis, J. Guertin, and D. M. Cottrell, "Diffraction-free beams generated with programmable spatial light modulators," Appl. Opt. **32**, 6368 (1993).

32. Y. Wang, W. Qu, L. Jiao, and Y. Zhang, "Generation and control of Bessel beams based on annular reflections," Appl. Phys. B **119**, 241 (2015).

33. Y. Xiao, L. Zhou, and W. Chen, "High-resolution ghost imaging through complex scattering media via a temporal correction," Opt. Lett. **47**, 3692 (2022).

34. B. G. Kitchener, J. Wainwright, and A. J. Parsons, "A review of the principles of turbidity measurement," Prog. Phys. Geog. **41**, 620 (2017).

35. Z. Sun, F. Tuitje, and C. Spielmann, "Toward high contrast and high-resolution microscopic ghost imaging," Opt. Express **27**, 33652 (2019).

36. Z. Sun, F. Tuitje, and C. Spielmann, "Improving the contrast of pseudothermal ghost images based on the measured signal distribution of speckle fields," Appl. Sci. **11**, 2621 (2021).